Image-charge forces in thin interlayers due to surface charges in electrolyte

Kirill A. Emelyanenko, Alexandre M. Emelyanenko, and Ludmila Boinovich*
A. N. Frumkin Institute of Physical Chemistry and Electrochemistry, Russian Academy of Sciences, Leninsky Prospect 31 Building 4, 119071 Moscow, Russia
(Received 27 November 2014; published 3 March 2015)

The surface forces arising in wetting films of nonpolar liquids or in thin air interlayers between an electrolyte and a nonpolar medium in the case of discrete charging of the dielectric-electrolyte interface are considered. The contributions of polarization effects to the distribution of the electrostatic potential in the three contacting media were calculated. Within the Debye-Hückel approximation, the analytical solutions were derived for the disjoining pressure in thin films, for the case of either dilute or relatively concentrated electrolyte solutions in the aforementioned systems. Analysis of the analytical and numerical results demonstrated that for dilute solutions the contribution of image forces to the disjoining pressure may significantly exceed the van der Waals forces for films from a few to tens of nanometers thick.

DOI: 10.1103/PhysRevE.91.032402 PACS number(s): 68.15.+e, 68.05.−n, 68.43.−h, 82.70.−y

I. INTRODUCTION

Interfaces are usually charged. The surface charge arises due to preferential transfer of a particular type of ion either from the bulk part of the contacting phases to the interface, or from the interfaces to the bulk phases, or, finally, due to ion exchange between the interfacial region and the bulk parts of the contacting phases. The first process is realized when different types of ions have different adsorbability from the solution to the interface. The dissociation of surface groups leads to processes of the second kind, when the surface acquires a charge with a sign determined by the nature of the ionogenic group. Finally, a third kind of process is possible. It is associated with a heterovalent isomorphic substitution of ions in the interfacial layer of one phase by the ions from an adjacent ionic solution.

In systems containing thin liquid interlayers, such as wetting or emulsion films, liquid-filled nanopores, or interlayers between particles of dispersed phase, charging of the interfaces causes additional polarization effects and formation of surface forces with an electrostatic origin. The study of phenomena related to interface charging is of considerable interest for both basic research and practical applications. Extensive studies in this area have been conducted for decades [1–7]. The focus in the theoretical studies of recent decades was on the systems important for colloid physics, biophysics, or biochemistry, in which the charges are located either in the vicinity of a single interface between bulk electrolyte and dielectric phases, or in the nanosize films of electrolytes, or, finally, in the dielectric interlayers confined (at least on one boundary) by an electrolyte solution [8–20].

In the aforementioned systems, phenomena related to polarization of the interfaces and to the discreteness of charges begin to play a key role. It is usually convenient to describe polarization of the interfaces by introducing image charges. For spatially confined systems with curved interfaces or for two closely located plane interfaces (for thin interlayers), an accurate description of polarization requires the introduction of an infinite series of image charges. In addition, for nanosized systems, the effect of charge discreteness becomes very appreciable, causing a significant deviation of system properties compared to those predicted on the assumption of uniform charge distribution. This deviation is most noticeable at the scale of several atomic distances around the charge location. As shown in numerous papers [12,13,18,20–23], charge discreteness affects the electric potential distribution in the vicinity of interfaces, diffusion and overcharging processes at the interfaces, the disjoining pressure in liquid interlayers, and the aggregation kinetics in dispersions.

Thus, Zhou [21] has shown that accounting for the discreteness of charge at dielectric surfaces immersed in an electrolyte solution gives a significant correction for the energy of interaction between two plates separated by an electrolyte interlayer. Monte Carlo simulations accounting for image charges [22–24] have shown that discrete charge distribution around spherical dielectric particles immersed in electrolyte drastically increases surface overcharging and affects the spatial distribution of the electric potential, especially in the case of multivalent electrolytes. Ions located in the vicinity of spherical particles induce an infinite number of image charges, and the contributions from the high-order images abruptly increase as the ions approach the particle surface. In this system, as well as in the case of a charge in the vicinity of a thin plane-parallel interlayer, correct calculation of the contributions from the high-order images becomes critical. The question of the physically reasonable number of contributions ensuring the appropriate estimate of excess energy of image charges is similar to the one arising in calculations of many-body contributions to the energy of van der Waals interactions between the nanoparticles or in thin interlayers [25,26].

The analysis of image forces in systems where the charges are located in ionic liquids or an aqueous electrolyte solution in the vicinity of a thin dielectric layer confined between the electrolyte and semi-infinite dielectric medium is an extremely interesting and practically important issue in the theory of stability of colloids and thin liquid films. A water droplet on a substrate is a typical example of such a system with wide practical applications. When the droplet is deposited onto the substrate, an air interlayer is formed between the droplet and the substrate at the moment of contact. In further evolution,

*Corresponding author: boinovich@mail.ru

this interlayer may either thin out and rupture for hydrophilic substrates or remain stable for superhydrophobic surfaces. A distinctive feature of the aforementioned system is that the polarization effects and electrostatic forces acting in the thin interlayers are effectively screened due to diffuse ionic clouds dressing the real charges in the electrolyte medium.

In this work, we consider the surface forces arising in wetting films of nonpolar liquids or in thin air interlayers between an electrolyte and a nonpolar medium in the case of discrete charging of the dielectric-electrolyte interface. We obtain analytical solutions for the disjoining pressure in a thin interlayer for a random ensemble of discrete surface charges located in the dilute or concentrated electrolyte solution. Finally, we show that for the systems of interest, the contribution of image forces to the disjoining pressure of the dielectric interlayer may significantly exceed the contributions from other types of surface forces.

II. CHARGED INTERFACE

A. Electrostatic potential induced by a point charge located in the electrolyte phase close to the interface in a bulk dielectric medium–dielectric film–electrolyte solution system

The model system containing an interlayer with dielectric permittivity ε_1 and thickness h, confined by two semi-infinite media with dielectric permittivities ε_2 and ε_3, is depicted in Fig. 1.

Medium 2 is an aqueous electrolyte solution, whereas media 1 and 3 are dielectric. The point charge q that appears due to charging of the electrolyte-dielectric interface is located within the electrolyte medium at distance z_0 from the position of the interface. We will consider the resulting electrostatic fields in the Cartesian coordinate system with the origin coinciding with the charge position and the z axis normal to the interface (Fig. 1). On one hand, the charge induces polarization of the interfaces, and on the other hand, the formation of a diffuse ionic atmosphere from electrolyte ions in the electrolyte solution. The electric potential distribution in the contacting media is described on the basis of the Poisson equation:

$$\begin{aligned}
&\Delta\phi^{(1)} = 0 \quad z_0 < z < (z_0 + h)\\
&\Delta\phi^{(2)} = -\frac{4\pi}{\varepsilon_2}[q\delta(x,y,z) + \rho(x,y,z)] \quad z < z_0 \qquad (1)\\
&\Delta\phi^{(3)} = 0 \quad z > (z_0 + h),
\end{aligned}$$

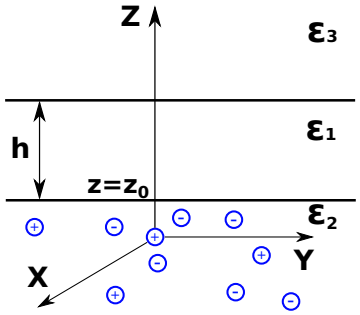

FIG. 1. (Color online) Point charge in the electrolyte close to the interface with a dielectric film.

where z_0 and $z_0 + h$ are positions of the interfaces separating the film from confining phases 2 and 3, respectively, and $\delta(x,y,z)$ is the Dirac delta function. The bulk charge density in the electrolyte may be related to the local concentration of ions, n_i, bearing the charge ez_i each (where e is the elementary charge, and z_i is the valence of the ion) by the evident relation

$$\rho = \sum_i ez_i n_i. \qquad (2)$$

Within the Debye-Hückel approximation valid for moderate electric fields ($e\phi \ll kT$), the ion density is proportional to the electrostatic potential $\phi^{(2)}$ inside the solution. Thus the electrostatic potential in all contacting media is described by the following set of Poisson-Boltzmann equations:

$$\begin{aligned}
&\Delta\phi^{(1)} = 0 \quad z_0 < z < (z_0 + h)\\
&\Delta\phi^{(2)} - \kappa^2\phi^{(2)} = -\frac{4\pi}{\varepsilon_2}q\delta(x,y,z) \quad z < z_0 \qquad (3)\\
&\Delta\phi^{(3)} = 0 \quad z > (z_0 + h),
\end{aligned}$$

with boundary conditions

$$\begin{aligned}
&z \to \infty \quad \phi^{(3)} \to 0\\
&z \to -\infty \quad \phi^{(2)} \to 0\\
&z = z_0 + h \quad \phi^{(1)} = \phi^{(3)}\\
&z = z_0 + h \quad \frac{\varepsilon_1\partial\phi^{(1)}}{\partial z} = \frac{\varepsilon_3\partial\phi^{(3)}}{\partial z} \qquad (4)\\
&z = z_0 \quad \phi^{(1)} = \phi^{(2)}\\
&z = z_0 \quad \frac{\varepsilon_1\partial\phi^{(1)}}{\partial z} = \frac{\varepsilon_2\partial\phi^{(2)}}{\partial z},
\end{aligned}$$

where $\kappa^2 = n_0\frac{4\pi e^2(z_+^2 + z_-^2)}{\varepsilon_2 kT}$, n_0 is the number concentration of dissociated molecules, and z_+ and z_- are valences of cations and anions, respectively.

Given the cylindrical symmetry of the system under consideration it is expedient to proceed to the cylindrical coordinate system ρ, φ, z and use a Hankel transform, which reduces the initial system to the system of differential equation with two variables λ, z, where λ is integrally conjugated with $\rho = \sqrt{x^2 + y^2}$.

$$\begin{aligned}
&\frac{d^2 f^{(1)}(\lambda,z)}{dz^2} - \lambda^2 f^{(1)}(\lambda,z) = 0 \quad z_0 < z < z_0 + h\\
&\frac{d^2 f^{(2)}(\lambda,z)}{dz^2} - (\kappa^2 + \lambda^2) f^{(2)}(\lambda,z) = -\frac{2q}{\varepsilon_2}\delta(z) \quad z < z_0 \qquad (5)\\
&\frac{d^2 f^{(3)}(\lambda,z)}{dz^2} - \lambda^2 f^{(3)}(\lambda,z) = 0 \quad z > z_0 + h.
\end{aligned}$$

By solving the above system with boundary conditions, Eq. (4), we find the following relations for the Hankel transforms of the potential in the contacting media:

$$\begin{aligned}
f^{(1)}(\lambda,z) = \frac{2q}{\lambda\varepsilon_1 + \xi\varepsilon_2}\frac{\exp[2\lambda(z_0 + h)] + \beta_{13}\exp(2\lambda z)}{[\exp(2\lambda h) - \beta'_{12}\beta_{13}]}\\
\times \exp\big(-\lambda(z + z_0) - \xi z_0\big)
\end{aligned}$$

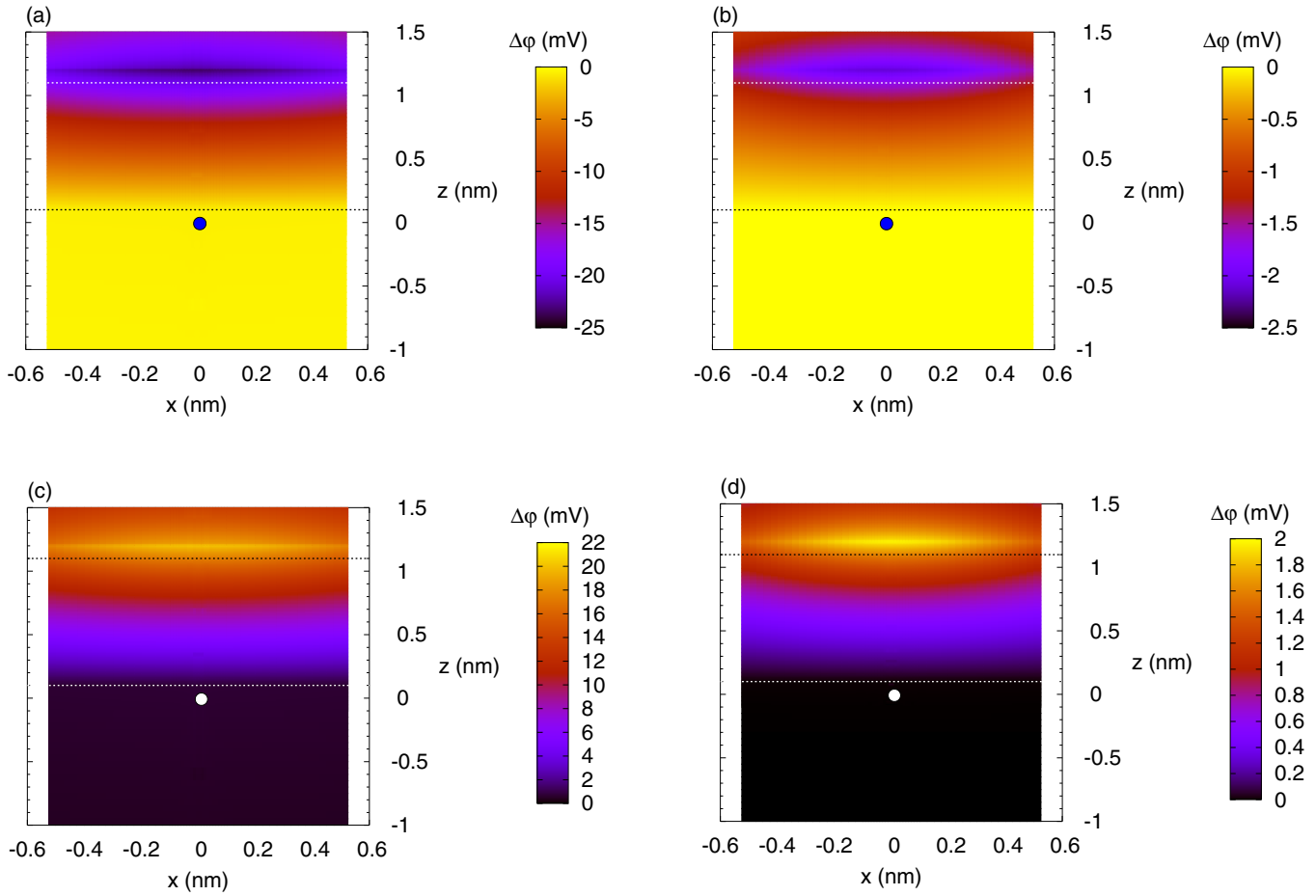

FIG. 2. (Color online) Potential maps illustrating the difference between the values of the electrostatic potential in the bulk dielectric–dielectric thin film–electrolyte solution and the appropriate reference systems. We used different reference systems for different areas of each map. Maps (a) and (b) were calculated for the 1-nm-thick air interlayer ($\varepsilon_1 = 1$) separating the bulk dielectric liquid ("oil", $\varepsilon_3 = 2$) from an aqueous 1-1 electrolyte solution, with bulk air–electrolyte reference system for air interlayer and electrolyte region, and bulk oil–electrolyte system as a reference for oil region. Maps (c) and (d) were calculated for an oil ($\varepsilon_1 = 2$) wetting film 1 nm thick on the surface of an aqueous 1-1 electrolyte solution, with the air ($\varepsilon_3 = 1$) surrounding medium. For latter maps, bulk air–electrolyte reference system was used for air half space, and bulk oil/electrolyte was a reference for oil and electrolyte regions. The parameters of electrolyte solutions were $\varepsilon_2 = 80$ and $\kappa = 10^{-3}\,\mathrm{nm}^{-1}$ for dilute solution [maps (a) and (c)] and $\varepsilon_2 = 40$ and $\kappa = 10\,\mathrm{nm}^{-1}$ for concentrated solution [maps (b) and (d)]. Points indicate the charge location, and dashed lines correspond to positions of interlayer boundaries.

$$f^{(2)}(\lambda,z) = \frac{q}{\xi\varepsilon_2}\{\exp(-\xi|z|) - \beta'_{12}\exp[\xi(z-2z_0)]\} + \frac{4q\lambda\varepsilon_1\beta_{13}}{(\lambda\varepsilon_1+\xi\varepsilon_2)^2}\frac{\exp[\xi(z-2z_0)-2\lambda h]}{\{1-\beta'_{12}\beta_{13}\exp(-2\lambda h)\}}$$
$$f^{(3)}(\lambda,z) = \frac{2q}{\lambda\varepsilon_1+\xi\varepsilon_2}\frac{(1+\beta_{13})\exp(\lambda z_0-\xi z_0+2\lambda h-\lambda z)}{[\exp(2\lambda h)-\beta'_{12}\beta_{13}]}, \quad (6)$$

where $\xi = \sqrt{\lambda^2+\kappa^2}$; $\beta'_{12} = (\lambda\varepsilon_1-\xi\varepsilon_2)/(\lambda\varepsilon_1+\xi\varepsilon_2)$; $\beta_{13} = (\varepsilon_1-\varepsilon_3)/(\varepsilon_1+\varepsilon_3)$.

The inverse Hankel transform of Eq. (6) allows us to obtain the corresponding expressions for electric potential distribution, $\phi^{(i)}(x,y,z)$, in the Cartesian coordinate system. In general, the analytical expressions for the inverse transforms of Eq. (6) do not exist for an arbitrary set of system parameters. At the same time, the potentials $\phi^{(i)}(x,y,z)$ can be computed numerically for any given values of the system parameters. In this context, the evaluation of excess potential associated with the geometry of the system is of particular interest. We calculated the difference in the values of the electrostatic potential in the bulk dielectric–dielectric thin film–electrolyte solution and bulk dielectric–electrolyte solution systems. This calculation allows us to estimate the cross contributions of the two closely spaced boundaries to the value of the potential in the three contacting media. In other words, in this calculation we obtain the total contribution to the magnitude of the potential $\phi^{(i)}$ from all but the first-order images of the charge under consideration.

In Fig. 2 we present the results of these calculations for the air interlayer separating the bulk dielectric liquid from a concentrated (a) or dilute (b) aqueous 1-1 electrolyte solution, as well as for a dielectric wetting film 1 nm thick on the surface of an aqueous 1-1 electrolyte solution for a concentrated (c) and dilute (d) solution. The reference system is bulk electrolyte–air for the electrolyte phase in (a) and (b) maps, and for air phases in all maps; and bulk electrolyte–bulk dielectric liquid for the electrolyte phase in (c) and (d) maps,

and for dielectric liquid phases in all maps. It worth noting that the potential maps presented in Fig. 2 provide an explicit visualization of the electric fields of image charges in stratified media and an estimation of the role of high-order images.

At the same time, for a number of practically important values of parameters for this system, Eq. (6) for $f^{(2)}(\lambda,z)$, which is required for further analysis of thin film stability, can be reduced to a form suitable for analytical inverse Hankel transform without loss of calculation accuracy.

It should be emphasized here that the analytical representation of the potential distribution in medium 2, and its dependence on the system parameters, is necessary for a detailed analysis of the influence of interface charging on the stability and energy of a thin dielectric layer. Since in what follows we will only be interested in the film thickness–dependent part of the electrostatic potential, we will distinguish the term that depends on h in Eq. (6):

$$f_h^{(2)}(\lambda,z) = \frac{4q\lambda\varepsilon_1\beta_{13}}{(\lambda\varepsilon_1+\xi\varepsilon_2)^2}\frac{\exp[\xi(z-2z_0)-2\lambda h]}{\{1-\beta'_{12}\beta_{13}\exp(-2\lambda h)\}}. \quad (7)$$

Then for the thickness-dependent part of the potential $\phi_h^{(2)}(z,\rho)$ we obtain

$$\phi_h^{(2)}(z,\rho) = \int J_0(\rho\lambda)\lambda\frac{4q\lambda\varepsilon_1\beta_{13}}{(\lambda\varepsilon_1+\xi\varepsilon_2)^2} \times \frac{\exp[\xi(z-2z_0)-2\lambda h]}{\{1-\beta'_{12}\beta_{13}\exp(-2\lambda h)\}}d\lambda, \quad (8)$$

where $\rho=\sqrt{x^2+y^2}$.

We consider two limiting cases, $\kappa \gg 1/h$ and $\kappa \ll 1/h$, both permitting an analytical inverse Hankel transform for $\phi_h^{(2)}(z,\rho)$. The first limit corresponds to concentrated solutions in contact with dielectric films a few nanometers thick. The behavior of the integrand in Eq. (8) is determined by its exponential decay as $\exp(-2\lambda h)$, and the main contribution to the integral comes from the range $\lambda \in [0; n/h]$, with n of order of unity. Then for the case under consideration we can put

$$\lambda\varepsilon_1+\xi\varepsilon_2 \approx \kappa\varepsilon_2, \quad \beta'_{12} \approx -1, \quad (9)$$

Using these approximations and taking into account the identity

$$\frac{1}{1+\beta_{13}\exp(-2\lambda h)} = \sum_{k=0}^{\infty}(-\beta_{13})^k\exp(-2k\lambda h) \quad (10)$$

we can rewrite Eq. (8) as

$$\phi_h^{(2)}(z,\rho) = -\sum_{k=0}^{\infty}(-\beta_{13})^{k+1}\frac{4q\varepsilon_1}{{\varepsilon_2}^2} \times \int J_0(\rho\lambda)\frac{\lambda^2}{\kappa^2}\exp[\kappa(z-2z_0)-2\lambda(k+1)h]d\lambda. \quad (11)$$

The integral in Eq. (11) is expressed through the second-order Legendre polynomials. This leads to the following relation for the film thickness–dependent part of the electric potential within a nanosize dielectric film on the surface of a concentrated electrolyte solution:

$$\phi_h^{(2)}(z,\rho) = -\sum_{k=0}^{\infty}(-\beta_{13})^{k+1}\frac{4q\varepsilon_1}{\kappa^2{\varepsilon_2}^2}\exp[\kappa(z-2z_0)] \times \frac{8(k+1)^2h^2-\rho^2}{\{[2(k+1)h]^2+\rho^2\}^{5/2}}. \quad (12)$$

Note that mathematical procedure of fraction expansion into a series used in Eq. (10) has a clear physical meaning. Each term of the series in the resulting expansion, Eq. (12), describes the contribution of the corresponding-order image charge.

Now we consider the second limit, corresponding to dilute solutions and films that are not very thick, when the condition $\kappa \ll 1/h$ holds. In this case, the definitional domain of the integrand in Eq. (8) can be divided into sections $[0,\kappa n]$, $[\kappa n, m/h]$, and $[m/h,\infty]$, where m and n are numbers of the order of unity. Given that $\kappa \ll 1/\rho$, the magnitude of the integrand beyond the two first sections is small and decays fast [because of the factor $\exp(-2\lambda h)$]; hence, we may neglect the contribution from the last section to the total integral. The relation of contributions to the total integral from the two first sections can be estimated as

$$\frac{[0,\kappa n]}{[\kappa n, m/h]} \propto \frac{\kappa}{\frac{1}{h}} = \kappa h \ll 1. \quad (13)$$

Hence, we may neglect the contribution from the first section as well. Then without essential loss of accuracy, we can assume that the main contribution to the integral comes from the range $\lambda \gg \kappa$, and put

$$\lambda\varepsilon_1+\xi\varepsilon_2 \approx \lambda(\varepsilon_1+\varepsilon_2), \quad \beta'_{12} \approx \frac{\varepsilon_1-\varepsilon_2}{\varepsilon_1+\varepsilon_2} \equiv \beta_{12}. \quad (14)$$

Using approximations (14) and taking the identity (10) into account, we can integrate Eq. (8) to get

$$\phi_h^{(2)}(\rho,z) = \sum_{k=0}^{\infty}\frac{4q\varepsilon_1\beta_{13}^{k+1}\beta_{12}^k}{(\varepsilon_1+\varepsilon_2)^2} \times \frac{1}{\sqrt{\{[2h(k+1)-z+2z_0]\}^2+\rho^2}}. \quad (15)$$

To evaluate the accuracy of the derived analytical approximations for the thickness-dependent part of the electrostatic potential, we have calculated the values of $\phi_h^{(2)}(0,0)$ for various film thicknesses using approximate relations, Eqs. (12) and (15), and by direct numerical integration of Eq. (8). The relative deviations of the potentials calculated by analytical approximations from those computed numerically, shown in Fig. 3, substantiate the conclusion that the analytical relations obtained here for $\phi_h^{(2)}(\rho,z)$ accurately reproduce the thickness-dependent part of the electrostatic potential for the appropriate ranges of thicknesses satisfying the conditions $\kappa \gg 1/h$ or $\kappa \ll 1/h$.

B. Forces induced by an ensemble of discrete charges in a dielectric interlayer confined by bulk dielectric medium and electrolyte solution

Equations (12) and (15) derived above allow us to calculate the potential induced by a single charge in the electrolyte

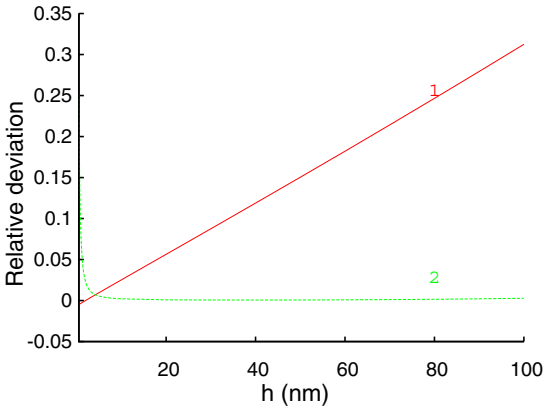

FIG. 3. (Color online) The relative deviations of the potentials calculated by analytical approximations, Eq. (15) for $\kappa h \ll 1$ (line 1), and Eq. (12) for $\kappa h \gg 1$ (line 2), from those computed by numerical integration of Eq. (8).

medium, with consideration of the polarization effects at the interfaces. However, in real systems, interface charging involves the formation of the ensemble of charges at the interface. The lateral positions of these charges are disordered, first of all because of the thermal motion of ions. We will use the cut-out disk method [12,13,27–29] to calculate the electric potential induced by a whole ensemble of charged entities in the electrolyte medium. In this method, summation over an infinite number of discrete randomly distributed charges is replaced by integration over the surface with averaged charge density. The charge density around the chosen point charge is approximated in the model by a step function

$$\sigma(\rho) = \begin{cases} 0 & 0 < \rho < \rho_0 \\ \sigma = q/\pi\rho_0^2 & \rho_0 < \rho < \infty \end{cases}, \qquad (16)$$

where $\pi\rho_0^2$ is the average area per charge in the adsorption layer. Then the full potential of the electric field, $\phi_\Sigma^{(2)}$ induced at the location of a given adsorbed charge by all the other real adsorbed charges and by all the image charges can be calculated as

$$\phi_\Sigma^{(2)}(0,0) = \phi_0(0,0) + \frac{2}{\rho_0^2}\int_{\rho_0}^{\infty} \phi(\rho,0)\rho d\rho, \qquad (17)$$

where $\phi_0(0,0)$ is the potential of the field induced by all the images of the given charge, and $\phi(\rho,0)$ is the potential induced by a point charge at a distance ρ from the given charge and by all its images. Combining Eqs. (17) and (12), we get the following relation for the thickness-dependent part of the potential in the concentrated electrolyte solution:

$$\phi_\Sigma^{(2)}(0,0) = -\sum_{k=0}^{\infty} (-\beta_{13})^{k+1} \frac{q\varepsilon_1}{\kappa^2 {\varepsilon_2}^2} \exp[-2\kappa z_0] \times \left[\frac{1}{(k+1)^3 h^3} - \frac{8}{\left[4(k+1)^2 h^2 + \rho_0^2\right]^{3/2}}\right]. \qquad (18)$$

The thickness-dependent part of the potential electric energy for the monolayer of charges adsorbed in medium 2 at the (2-1) interface is calculated as the product of the magnitude of adsorption, $\Gamma^{(21)}$ at that interface on the corresponding part of the potential energy of a single charge in the electric field induced by other real adsorbed charges and by all the image charges. Therefore, for the contribution of image forces to the disjoining pressure of interlayer 1 we can write

$$\Pi_{\text{image}} = -\frac{dU}{dh} = -\frac{d(q\phi_\Sigma)}{dh}\Gamma^{(21)}. \qquad (19)$$

From Eqs. (18) and (19), and given that $\Gamma^{(21)} = 1/\pi\rho_0^2$, we obtain the expression for the image-charge component for the disjoining pressure in a dielectric film confined by bulk dielectric and concentrated electrolyte solution:

$$\Pi_{\text{image}}(h) = \sum_{j=1}^{\infty} (-\beta_{13})^j \frac{q^2\varepsilon_1}{\kappa^2 {\varepsilon_2}^2} \exp[-2\kappa z_0] \frac{1}{\pi {\rho_0}^2} \times \left[\frac{-3}{j^3 h^4} + \frac{96 h j^2}{\left(4j^2h^2 + \rho_0^2\right)^{5/2}}\right]. \qquad (20)$$

Recall that Eq. (20) was derived under the condition $\kappa \gg 1/h$; therefore, its applicability to films with a thickness of several monolayers (i.e., on the order of 1 nm) is justified for solutions of symmetric 1-1 electrolyte with concentration greater than $1M$. Such solutions can be treated in the frame of the Debye-Hückel approximation for the case of insignificant ion-ion correlations only. Although the constraint on the solution concentration becomes somewhat milder as film thickness increases, strictly speaking, Eq. (20) still remains valid only in relatively concentrated electrolytes.

By analogy with the derivation for concentrated solutions presented above, we can combine Eqs. (17) and (15), and performing first a differentiation over film thickness (to avoid divergence) and then an integration over ρ, to get

$$\Pi_{\text{image}} = \sum_{k=0}^{\infty} \frac{4q^2\varepsilon_1\beta_{13}^{k+1}\beta_{12}^k}{(\varepsilon_1+\varepsilon_2)^2} \frac{1}{\pi\rho_0^2}(k+1) \times \left(\frac{1}{2\{[h(k+1)+z_0]\}^2} + \frac{4}{\rho_0^2} \frac{\{[2h(k+1)+2z_0]\}}{\sqrt{\{[2h(k+1)+2z_0]\}^2 + \rho_0^2}}\right). \qquad (21)$$

As mentioned above, for sufficient strictness of Eq. (21), the restriction $\kappa \ll 1/h$ must hold. For 1-nm-thick films, this corresponds to dilute electrolyte solutions with concentration less than 10^{-3} M. As film thickness increases, the constraint on the low ion concentration becomes more and more strict. At the same time, for pure water, where Debye length is on the order of one hundred nanometers, Eq. (21) works satisfactorily for the wide range of thicknesses up to several tens of nanometers.

III. CONTRIBUTION OF IMAGE FORCES TO THE STABILITY OF THIN AIR INTERLAYERS AND WETTING FILMS

The values of the disjoining pressure calculated by Eqs. (20) and (21) determine the contribution of image forces to the total disjoining pressure of a thin dielectric interlayer separating the bulk electrolyte phase and the dielectric. To assess the role of this type of surface force in the stability of thin interlayers, we have calculated the isotherms $\Pi_{\text{image}}(h)$ for wetting films of oil

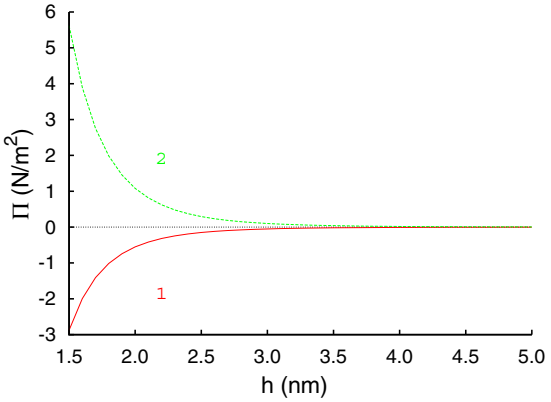

FIG. 4. (Color online) Contribution of image forces to the disjoining pressure of (1) air interlayer between an electrolyte solution and a dielectric liquid, and (2) dielectric wetting film on surface of electrolyte solution. The calculations were performed for a concentrated electrolyte solution using Eq. (20) with the following values of system parameters: $\varepsilon_2 = 40$; $\kappa = 10\,\mathrm{nm}^{-1}$; $\sigma = 0.05\,\mathrm{C\,m}^{-2}$; $z_0 = 0.1\,\mathrm{nm}$; $\varepsilon = 2$ for dielectric liquid.

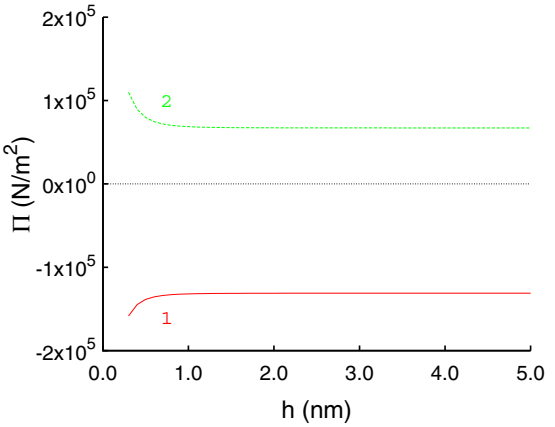

FIG. 5. (Color online) Contribution of image forces to the disjoining pressure of (1) air interlayer between an electrolyte solution and a dielectric liquid, and (2) dielectric wetting film on surface of electrolyte solution. The calculations were performed for a dilute electrolyte solution using Eq. (21) with the following values of system parameters: $\varepsilon_2 = 80$; $\kappa = 10^{-3}\,\mathrm{nm}^{-1}$; $\sigma = 0.05\,\mathrm{C\,m}^{-2}$; $z_0 = 0.1\,\mathrm{nm}$; $\varepsilon = 2$ for dielectric liquid.

on the surface of aqueous solutions and for the air interlayers between a drop of an aqueous solution and a substrate with a low dielectric constant. The results of calculations for a concentrated electrolyte solution are presented in Fig. 4.

Analysis of the data suggests that screening of the surface charge by an electric double layer in concentrated electrolyte with a low Debye length allows for effective weakening of the polarizing effect of the charge on the film interfaces. As a result, the magnitude of the contribution of image forces decreases rapidly with film thickness; for interlayers of nanometer thickness in both the aforementioned systems, it is as little as a few Newtons per square meter. The sign of Π_{image} does not depend on the sign of the charge, and is determined by the relation between the dielectric constants of the contacting media. Thus, the image forces induce a destabilizing effect on air interlayers, contributing to their breakthrough. Conversely, for oil films the image forces induced by discretely charged electrolyte-oil interface promote film stabilization.

Now consider the case of a dilute electrolyte. As follows from Eq. (21), the isotherm of the disjoining pressure is defined by two terms that have different character of dependence on film thickness. For films with a thickness on the order of a few molecular layers, the prevailing contribution comes from the first term decaying as the inverse square of the film thicknesses. However, for film thicknesses greater than 2 nm, the contribution from the second term starts to dominate. This term is almost independent of thickness. This independence should not confuse the reader, since it is necessary to keep in mind that Eq. (21) is valid only for those thicknesses for which $\kappa \ll 1/h$. For any arbitrary electrolyte concentration (in other words, for any fixed k) this condition breaks down with an increase in thickness, and for large film thicknesses ($\kappa \gg 1/h$) the disjoining pressure vanishes as $1/h^4$ according to Eq. (20). The results of the calculation (Fig. 5) show that for dilute electrolyte solutions the contribution of image forces to the disjoining pressure is very significant for both the wetting dielectric films and for the air interlayers. Again, as in the case of concentrated solutions, these forces contribute to stabilization of wetting films and promote the rupture of air interlayers.

As follows from Eqs. (20) and (21), one of the key parameters affecting the magnitude of the contribution of image forces to the stability of thin layers is the area per unit charge at the interface. Charging of aqueous solution–oil and aqueous solution–gas interfaces can be flexibly varied by changing either the pH of the aqueous solution or salt concentration [30]. The results of calculations of the effect of the surface charge density, σ_{so}, at the solution-oil interface (or, in other words, of the average distance between the charges at that interface, ρ_{so}) on the contribution of image forces to the disjoining pressure of the oil wetting film on the surface of 1-1 electrolyte are presented in Fig. 6. Analysis of Eq. (21) and the data presented indicates a very steep increase in the disjoining

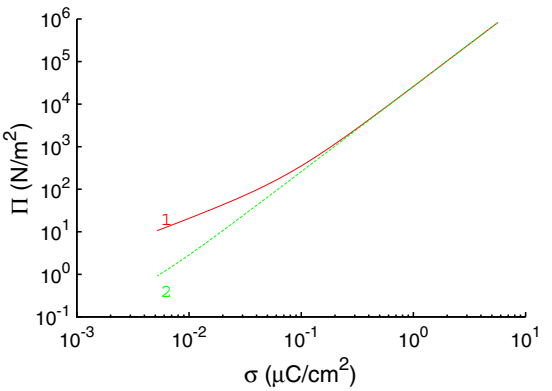

FIG. 6. (Color online) Dependence of image forces contribution to the disjoining pressure on the density of surface charges. The calculations were performed for dielectric wetting film with thickness of (1) 1 nm and (2) 5 nm, on a surface of a dilute electrolyte solution, using Eq. (21) with the following values of system parameters: $\varepsilon_2 = 80$; $\kappa = 10^{-3}\,\mathrm{nm}^{-1}$; $z_0 = 0.1\,\mathrm{nm}$; $\varepsilon_1 = 2$.

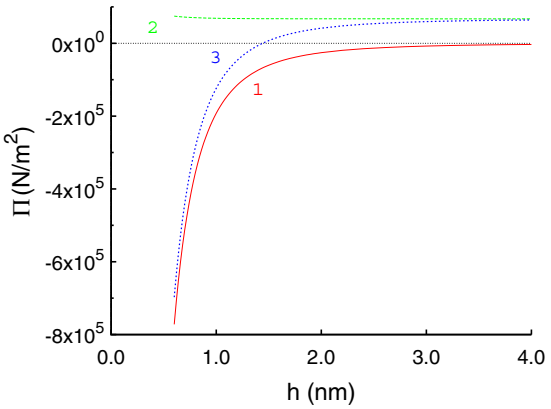

FIG. 7. (Color online) The isotherms of van der Waals (1) and image-charge (2) contributions to the total disjoining pressure (3) of heptane wetting film on the water surface. The calculations of image-charge forces were performed using Eq. (21) with the following values of system parameters: $\varepsilon_1 = 1.923$; $\varepsilon_2 = 80$; $\varepsilon_3 = 1$; $\kappa = 10^{-3}\,\mathrm{nm}^{-1}$; $z_0 = 0.1\,\mathrm{nm}$; $\sigma = 0.05\,\mathrm{C\,m}^{-2}$; the van der Waals forces were calculated as described in [13].

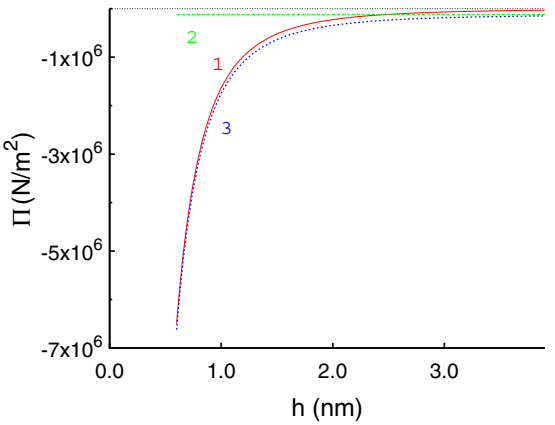

FIG. 8. (Color online) The isotherms of van der Waals (1) and image-charge (2) contributions to the total disjoining pressure (3) of air interlayer separating bulk heptane and water phases. The calculations of image-charge forces were performed using Eq. (21) with the following values of system parameters: $\varepsilon_1 = 1$; $\varepsilon_2 = 80$; $\varepsilon_3 = 1.923$; $\kappa = 10^{-3}\,\mathrm{nm}^{-1}$; $z_0 = 0.1\,\mathrm{nm}$; $\sigma = 0.05\,\mathrm{C\,m}^{-2}$; the van der Waals forces were calculated as described in Ref. [13].

pressure with a decrease in the average distance between charges: For small thicknesses $\Pi_{\mathrm{image}}(h)$ is proportional to the surface charge density, while for thicker films it scales as the square of the charge density.

So far, we have only discussed the contribution of image forces to the disjoining pressure of a thin interlayer. However, the stability of wetting films or thin interlayers is determined by the concurrent action of surface forces with various origins. The van der Waals forces are the most ubiquitous ones present in any system. In the systems analyzed here, charging takes place at only one of the two film interfaces; thus, there is no electrostatic interaction of the real charges located on the opposite boundaries. We will also neglect the image forces associated with a diminutive solubility of water in oil films [13].

For a comparative analysis of the contribution of forces of different nature to the stability of the films, we have calculated the total disjoining pressure in a wetting oil film on the water surface and in the air interlayer between the oil and water at a temperature of 20 °C. The van der Waals forces were calculated on the basis of the method and the experimental data presented in [13,31]. Figure 7 shows the results of calculations for heptane films on the water surface. For this system, the negative sign of the van der Waals forces (line 1) contributes to the destabilization of the film. In contrast, the contribution of the image forces (line 2) is positive. When film thickness is about 1 nm, the first type of force prevails, leading to the instability of heptane films less than 1.5 nm thick (line 3). However, due to faster decay of the van der Waals forces compared to the image forces for dilute solutions, the stabilization of thicker films is possible due to the image forces effect.

For air interlayers (Fig. 8), both types of forces lead to a negative disjoining pressure, mutually reinforcing instability of the air gap. However, while the contribution of image forces for a film 1 nm thick is on the order of 10% of the total disjoining pressure, for $h > 3\,\mathrm{nm}$ this contribution becomes dominant. Specifically, the image forces should determine the features of the displacement of air cushions formed between an aqueous droplet and a substrate with low dielectric constant.

IV. CONCLUSIONS

Despite considerable advances in the theory of surface forces, some important application-specific problems still require theoretical study. In particular, more detailed analysis is needed to better understand the forces that determine the behavior of thin air interlayers arising in the contact between an aqueous droplet and a substrate [32–34]. The study of surface forces acting in thin wetting films of oil on the surface of aqueous electrolyte solutions will further the advancement in solving the problem of separating oil-water emulsions or cleaning oil slicks from the surface of natural water basins. The analysis performed in this work indicates that image forces may play a key role in either stabilizing or thinning out thin interlayers for both the air gaps and the oil wetting films.

In the aforementioned systems, the charges are located within aqueous electrolyte solutions close to the interface with a thin dielectric interlayer separating the electrolyte from another bulk dielectric medium. The distinctive feature of this system is substantial screening of both the polarization effects and the electrostatic forces in thin interlayers due to the formation of diffuse ionic atmospheres, which obscure the surface charges in the electrolyte. In addition, the discrete character of surface charge leads to uneven distribution of electrostatic potential in contacting media. Within the Debye-Hückel approximation, we have derived analytical solutions for the disjoining pressure in thin films, for the case of either dilute or concentrated electrolyte solutions in the aforementioned systems. Analysis of the analytical and numerical results obtained here leads to the conclusion that for dilute solutions, the contribution of image forces to the disjoining pressure may significantly exceed the van

der Waals forces for films a few nanometers thick. This dominance of image forces would undoubtedly be especially important for interlayers tens of nanometers thick. However, the relations derived in this work are only correct for thicker films as long as the condition holds that film thickness is much less than the Debye length in the electrolyte solution.

ACKNOWLEDGMENTS

This research was supported by the Presidential program of support for the Leading Scientific Schools (Project No. NSh-2181.2014.3). The calculations reported in this paper were performed using the supercomputer facilities of the "Lomonosov" and SKIF MSU "Chebyshev" systems of Moscow State University Supercomputing Centre.

[1] B. V. Derjaguin, N. V. Churaev, and V. M. Muller, *Surface Forces* (Consultants Bureau, New York, 1987).
[2] J. Israelachvili, *Intermolecular and Surface Forces* (Academic Press, New York, 2011).
[3] B. V. Derjaguin, *Theory of Stability of Colloids and Thin Films* (Springer, Heidelberg, 1989).
[4] L. B. Boinovich, Usp. Khim. **76**, 510 (2007).
[5] A. Y. Grosberg, T. T. Nguyen, and B. I. Shklovskii, Rev. Mod. Phys. **74**, 329 (2002).
[6] M. M. Hatlo and L. Lue, Soft Matter **4**, 1582 (2008).
[7] L. Boinovich, Curr. Opin. Colloid Interface Sci. **15**, 297 (2010).
[8] L. Foret and A. Wurger, J. Phys. Chem. B **108**, 5791 (2004).
[9] T. Tang, C. Y. Hui, and A. Jagota, J. Colloid Interface Sci. **299**, 572 (2006).
[10] E. Wernersoon and R. Kjellander, J. Chem. Phys. B **125**, 154702 (2006).
[11] M. Seijo, S. Ulrich, M. Filella, J. Buffle, and S. Stoll, J. Colloid Interface Sci. **322**, 660 (2008).
[12] A. Emelyanenko and L. Boinovich, J. Phys.: Condens. Matter **20**, 494227 (2008).
[13] L. Boinovich and A. Emelyanenko, Adv. Colloid Interface Sci. **147-148**, 44 (2009).
[14] S. Buyukdagli, M. Manghi, and J. Palmeri, Phys. Rev. E **81**, 041601 (2010).
[15] Z. Y. Wang and Y. Q. Ma, J. Chem. Phys. **131**, 244715 (2009).
[16] A. Wynveen and F. Bresme, J. Chem. Phys. **133**, 144706 (2010).
[17] S. Buyukdagli, M. Manghi, and J. Palmeri, J. Chem. Phys. **134**, 074706 (2011).
[18] A. G. Cherstvy and R. G. Winkler, J. Phys. Chem. B **116**, 9838 (2012).
[19] M. Kanduc, A. Naji, J. Forsman, and R. Podgornik, J. Chem. Phys. **137**, 174704 (2012).
[20] W. Pezeshkian, N. Nikoofard, D. Norouzi, F. Mohammad-Rafiee, and H. Fazli, Phys. Rev. E **85**, 061925 (2012).
[21] S. Zhou, J. Chem. Phys. **140**, 234704 (2014).
[22] Z. Gan and Z. Xu, Phys. Rev. E **84**, 016705 (2011).
[23] Z. Gan, X. Xing, and Z. Xu, J. Chem. Phys. **137**, 034708 (2012).
[24] Z. Xu, Phys. Rev. E **87**, 013307 (2013).
[25] M. W. Cole, D. Velegol, H. Y. Kim, and A. A. Lucas, Mol. Simul. **35**, 849 (2009).
[26] K. A. Emelyanenko, A. M. Emelyanenko, and L. Boinovich, Chem. Lett. **41**, 1253 (2012).
[27] S. Levine, G. M. Bell, and D. Calvert, Can. J. Chem. **40**, 518 (1962).
[28] N. V. Grigoriev and V. S. Krylov, Russ. J. Electrochem. **4**, 763 (1968).
[29] L. B. Boinovich and A. M. Emelyanenko, Adv. Colloid Interface Sci. **104**, 93 (2003).
[30] J. K. Beattie, A. M. Djerdjev, and G. G. Warr, Faraday Discuss. **141**, 31 (2009).
[31] F. M. Shagieva and L. B. Boinovich, J. Chem. Phys. **138**, 214502 (2013).
[32] J. de Ruiter, J. M. Oh, D. van den Ende, and F. Mugele, Phys. Rev. Lett. **108**, 074505 (2012).
[33] Y. Liu, P. Tan, and L. Xu, J. Fluid Mech. **716**, R9 (2013).
[34] M. J. Thoraval and S. T. Thoroddsen, Phys. Rev. E **88**, 061001 (2013).